Supplementary Online Appendix

The Importance of Being Early? Anticipatory Cash Transfers for Flood-Affected Households

Ashley Pople, Ruth Hill, Stefan Dercon, and Ben Brunckhorst

S1. Supplementary tables

Table S1.1. Robustnessto alternate model specifications

	(1) Child food consumption	(2) Adult-food-consumption index	(3) Life satis-faction	(4) Pre-emptive actions	(5) Asset loss index	(6) Borrowing index	(7) Remit-tances	(8) Earning-potential index
Mauza fixed effects								
Intent-to-treat (ITT) effect	0.101***	0.037	0.178***	0.075***	−0.074***	−0.049	0.041	0.051*
	(0.032)	(0.029)	(0.030)	(0.027)	(0.028)	(0.033)	(0.030)	(0.028)
N	7,541	8,948	8,937	8,944	8,947	5,996	8,947	8,941
R^2	0.10	0.15	0.17	0.18	0.20	0.17	0.10	0.17
Union fixed effects								
ITT	0.083***	0.031	0.179***	0.069***	−0.099***	−0.047	0.032	0.083***
	(0.030)	(0.027)	(0.029)	(0.026)	(0.028)	(0.031)	(0.028)	(0.027)
N	7,633	9,036	9,025	9,032	9,035	6,105	9,035	9,029
R^2	0.04	0.09	0.10	0.10	0.13	0.09	0.04	0.11
Clustering by mauza								
ITT	0.101***	0.037	0.178***	0.075*	−0.074*	−0.049	0.041	0.051
	(0.037)	(0.038)	(0.047)	(0.040)	(0.039)	(0.036)	(0.032)	(0.032)
N	7,541	8,948	8,937	8,944	8,947	5,996	8,947	8,941
R^2	0.10	0.15	0.17	0.18	0.20	0.17	0.10	0.17
Winsorized (p95)								
ITT	0.101***	0.041	0.182***	0.094***	−0.055*	−0.055	0.041	0.060**
	(0.032)	(0.028)	(0.030)	(0.028)	(0.028)	(0.034)	(0.030)	(0.028)
N	7,541	8,948	8,937	8,944	8,947	5,996	8,947	8,941
R^2	0.10	0.14	0.17	0.18	0.19	0.17	0.10	0.17
No controls								
ITT	0.096***	0.043	0.184***	0.080***	−0.069**	−0.050	0.041	0.045
	(0.032)	(0.029)	(0.031)	(0.027)	(0.029)	(0.033)	(0.030)	(0.029)
N	7,541	8,948	8,937	8,944	8,947	5,996	8,947	8,941
R^2	0.09	0.12	0.16	0.18	0.18	0.15	0.09	0.12
Post-double selection method								
ITT	0.189***	0.078**	0.215***	0.088**	−0.064*	−0.000	0.042	0.058
	(0.043)	(0.038)	(0.040)	(0.035)	(0.037)	(0.044)	(0.038)	(0.038)
N	7,381	8,751	8,740	8,747	8,750	5,909	8,750	8,744

Source: Authors' analysis based on survey data.
Note: Standardized mean treatment effects are reported with robust standard errors in parentheses. Except when indicated, controls are age, gender, education level, household size, dependency ratio, house structure, receipt of United Nations Population Fund and Food and Agriculture Organization interventions, and land type. Mauza fixed effects are included, except when union fixed effects are indicated. The last panel reports estimates using the post-double-selection method (Belloni, Chernozhukov, and Hansen 2014) which uses the lasso estimator to select the controls. $^{*}p < 0.10$, $^{**}p < 0.05$, $^{***}p < 0.01$.

Table S1.2. Robustness of results when accounting for schooling and other forms of UN assistance

	(1) Child food consumption	(2) Adult food consumption index	(3) Life satis-faction	(4) Pre-emptive actions	(5) Asset loss index	(6) Borrowing index	(7) Remit-tances	(8) Earning-potential index
Mauza fixed effects								
Intent-to-treat (ITT) effect	0.101***	0.037	0.178***	0.075***	−0.074***	−0.049	0.041	0.051*
	(0.032)	(0.029)	(0.030)	(0.027)	(0.028)	(0.033)	(0.030)	(0.028)
N	7,541	8,948	8,937	8,944	8,947	5,996	8,947	8,941
R^2	0.10	0.15	0.17	0.18	0.20	0.17	0.10	0.17
Sample with no schooling								
ITT	0.130***	0.082**	0.234***	0.054	−0.059	−0.088*	0.008	0.014
	(0.045)	(0.040)	(0.042)	(0.036)	(0.039)	(0.049)	(0.041)	(0.039)
N	3,498	4,525	4,519	4,524	4,524	2,767	4,525	4,523
R^2	0.15	0.17	0.20	0.23	0.23	0.23	0.12	0.21
By support from United Nations								
ITT	0.096***	0.040	0.174***	0.074***	−0.075**	−0.019	0.064**	0.041
	(0.034)	(0.030)	(0.032)	(0.028)	(0.030)	(0.035)	(0.031)	(0.030)
ITT × United Nations Population Fund support	−0.072	0.100**	0.026	0.032	0.033	−0.048	0.048	0.040
	(0.047)	(0.042)	(0.044)	(0.036)	(0.038)	(0.045)	(0.049)	(0.042)
ITT × Food and Agriculture Organization support	−0.058	0.081	0.017	0.097**	0.068	−0.208***	0.004	−0.049
	(0.057)	(0.053)	(0.051)	(0.046)	(0.045)	(0.056)	(0.060)	(0.050)
N	7,541	8,948	8,937	8,944	8,947	5,996	8,947	8,941
R^2	0.10	0.15	0.17	0.18	0.20	0.17	0.10	0.17

Source: Authors' analysis based on survey data.
Note: The first panel shows the standardized mean treatment effects using the main specification. The second panel shows results when restricting the sample to those with no schooling. The third panel shows effects of the cash transfer for households not receiving any support from other sources, and the marginal effects for households receiving assistance from the United Nations Population Fund and Food and Agriculture Organization respectively. We control for the same covariates and mauza fixed effects used in the main analysis in all specifications. Robust standard errors were used to correct for heteroskedasticity. $^{*}p < 0.10, ^{**}p < 0.05, ^{***}p < 0.01$.

S2. Processing and validation of satellite flood data

*

S2.1. Methods

S2.1.1. Flood mapping with Sentinel-1 SAR

To estimate the extent of flooding over space and time, we first take freely available 10 m Sentinel-1 Synthetic Aperture Radar (SAR) imagery from the European Space Agency.[1] Sentinel-1 SAR data have frequently been applied to map flooding in recent literature, including in Bangladesh (Uddin, Matin, and Meyer 2019). SAR imagery is particularly useful for flood mapping as it can be captured even in the presence of cloud cover, unlike satellite imagery from optical sensors such as Landsat and MODIS. This is relevant for the area of interest in Bangladesh which has significant cloud cover during monsoon seasons. Water bodies can be identified from SAR imagery due to their dark appearance.

* We thank Leonardo Milano and Hannah Ker from the UN Office for the Coordination of Humanitarian Affairs's Centre for Humanitarian Data and MapAction for processing and analysis of the satellite flood data. See also https://ocha-dap.github.io/pa-anticipatory-action/analyses/bgd/docs/summary_flooding.html.

[1] https://dataspace.copernicus.eu/data-collections/copernicus-sentinel-missions/sentinel-1

The methodology used is adapted from the UN-SPIDER Knowledge portal and applies a change detection and thresholding (CDAT) approach to identify flooded areas.[2] The CDAT methodology for identifying flooded areas from Sentinel-1 data has been applied in contexts such as Bangladesh, Namibia, and the United Kingdom. The analysis was performed in the Google Earth Engine. The image processing methodology described below is largely summarized from the UN-SPIDER guidance.

S2.1.2. Image filtering and preprocessing

Th available Sentinel-1 imagery for the time period of interest is filtered according to the instrument mode, polarization, and pass direction. This filtering is necessary to ensure that mosaicked images share the same characteristics. The selected imagery has already undergone preprocessing steps to convert pixel values to their backscatter coefficients. These steps include thermal noise removal, radiometric calibration, and terrain correction, as well as applying a smoothing filter to reduce the speckle effect of radar imagery.[3]

S2.1.3. Change detection and thresholding to identify flooding

This methodology identifies flood extent by comparing imagery captured during flooding to baseline imagery without flooding for the area of interest. We took the median of all images from December 2019 to January 2020 from the area of interest to generate the baseline mosaic. We also checked the EM-DAT database to ensure that no floods were recorded during this period. The flood period mosaic is divided by the baseline mosaic, with pixel intensity in the resulting image indicating the degree of change between the two images. A threshold of 1.25 is applied to generate a binary layer indicating the full estimated extent of flooding. This threshold level is taken directly from the UN-SPIDER guidance, where it was selected "through trial and error." The appropriateness of this threshold level was also manually checked by comparing the derived flood extents with the satellite imagery for selected dates.

The flood extent output is further refined to mask the main water bodies and also to remove regions where the average slope is greater than 10 percent. Main water bodies are identified using the JRC Global Surface Water dataset, using a threshold of areas covered by water for at least 10 months in a year. Slope is calculated from the WWF HydroSHEDS DEM, based on SRTM data.

To understand the evolution of flooding over time, we repeated this change detection process separately on all available Sentinel-1 data for the area of interest between June and August 2020. In this case, 17 mosaicked images were available throughout this time period for our area of interest, generating a total of 17 output shapefiles that delineate flood extent for dates between June 2020 and August 2020, as shown in fig. S2.1.

The estimates of flood extent were then aggregated to a given admin unit (5,831 mauzas) by calculating the total flooded fraction within each unit for each point in time. Note that the area of permanent water bodies was removed from the area of each admin unit. The flooded fraction values thus represent the fraction of flooded area that is not normally covered by water.

While SAR imagery has commonly been used to map flooding, it is not without its limitations. As is well acknowledged within the literature, classification errors may arise in cases where water surfaces are roughened by wind or rain, and where other flat land surfaces (such as roads) are misclassified as water. Flood detection from SAR imagery is also poorer in urban areas and areas with dense, protruding vegetation. Results should also not be mistaken for any indication of flood depth, as only information about surface water coverage is captured by the satellite imagery.

S2.1.4. Interpolating and smoothing flooding estimates over time

As the temporal frequency of Sentinel-1 imagery can be up to 12 days between images, we cannot solely rely on the results of analyzing this imagery to accurately identify peak flooding dates. We therefore estimate the flooded fraction by admin unit at daily intervals by fitting the Sentinel-1 data points to a Gaussian function. The peak of the Gaussian curve for each admin unit was then used to identify the

[2] https://www.un-spider.org/advisory-support/recommended-practices/recommended-practice-google-earth-engine-flood-mapping/in-detail.
[3] https://developers.google.com/earth-engine/guides/sentinel1.

Figure S2.1 Dates of available Sentinel-1 satellite imagery against GloFAS water discharge measurements at Bahadurabad station

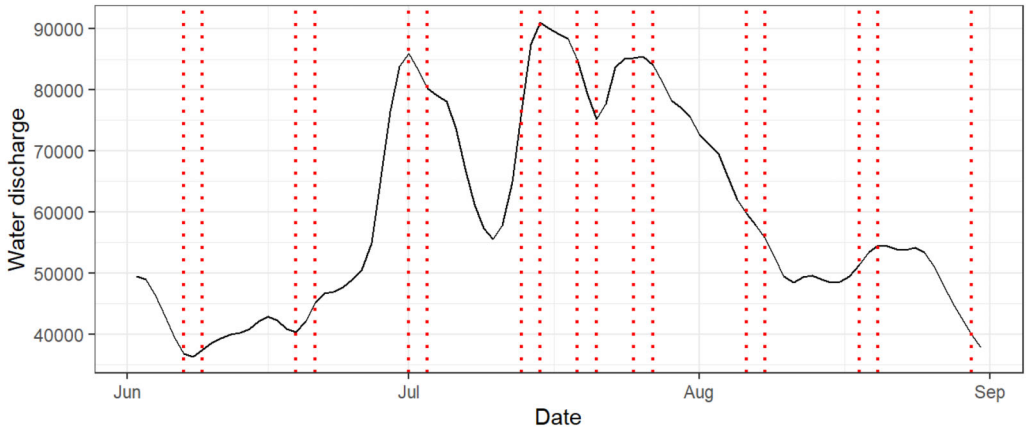

Source: Figure created by Hannah Ker (MapAction) on behalf of the Centre for Humanitarian Data, Office for the Coordination of Humanitarian Affairs, using Sentinel-1 SAR and GloFAS data.
Note: The figure shows the dates on which Sentinel-1 satellite imagery was available for the study area (red dotted vertical lines), plotted against GloFAS water discharge measurements at the Bahadurabad gauging station along the Jamuna River (solid black line), from June to September 2020. The imagery dates are used to estimate flood extent at the mauza level over the course of the 2020 monsoon flooding. Water discharge is measured in cubic metres per second.

estimated peak flooding date for that unit. This method simplifies the shape of the flooding time series and reduces the potential impacts from noise introduced by the limitations of the flooding estimates derived directly from the Sentinel-1 imagery.

It should be noted that a Gaussian function significantly simplifies the dynamics of flooding. By fitting to this function, we are making the assumption that the flooding extent within a mauza increased and decreased at the same rate, and the flooding had a single, distinct peak. These results should be considered as a best estimate of the flooding dynamics, based on the information available. A notable limitation of this current approach is that it does not capture multiple flooding peaks, as is known to have occurred in some regions of our study area. Mauzas where the Gaussian function fit was poor are flagged so they can be excluded from the analysis.

S2.2. Validation

S2.2.1. Comparison against the dynamics of GloFAS water discharge measurements

Figure S2.2 offers a comparison between GloFAS water discharge measurements at stations along the Jamuna River and the satellite-derived flooded fraction for the mauzas that contain those stations. While we should be careful directly comparing measurements of two different variables (flood extent and river water level), this visual comparison allows us to validate that the satellite-derived flooding fraction peaked at a similar time to when the nearby river water level peaked.

S2.2.2. Validating the flood extend against optical imagery

In the absence of ground-truth data, it is standard practice within the literature to validate Sentinel-1 derived flood extents against alternative sources of optical satellite imagery. However, obtaining cloud-free imagery to cover a large region, particularly during the rainy season in Bangladesh can be challenging. Nevertheless, we obtained Sentinel-2 imagery from 27 July, which provides a cloud-free look at some of the regions within our study area. We can visually compare this imagery against our output flood extent areas derived from Sentinel-1 SAR data from a similar date to check for agreement with areas that appear to be flooded, as demonstrated in fig. S2.3. While these images are only for a single date and for subsets of our study area, we see a clear agreement between flooded areas in the optical imagery (underlying layer and sole layer on the right) and the red overlaid flood extents from our Sentinel-1 analysis.

Figure S2.2 Comparison between flooding estimates against GloFAS water discharge measurements

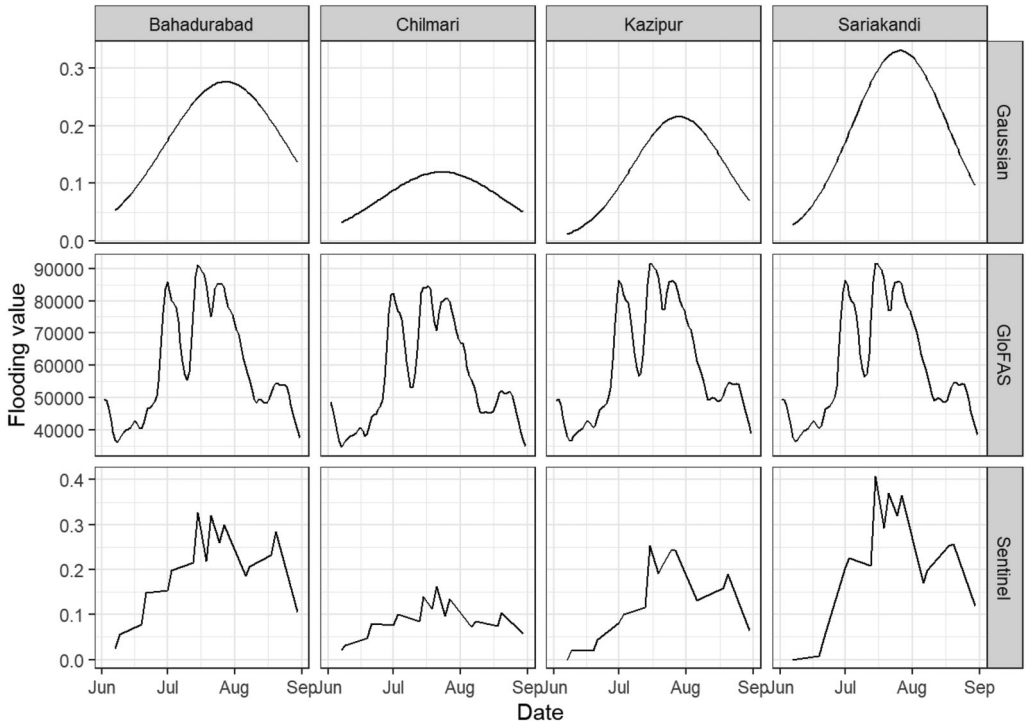

Source: Figure created by Hannah Ker (MapAction) on behalf of the Centre for Humanitarian Data, Office for the Coordination of Humanitarian Affairs, using Sentinel-1 SAR and GloFAS data.
Note: The figure compares satellite-derived flooding estimates against GloFAS water discharge measurements at four gauging stations along the Jamuna River — Bahadurabad, Chilmari, Kazipur, and Sariakandi — from June to September 2020. For each station, three panels are shown: the Gaussian-smoothed flood extent (top), GloFAS water discharge in cubic metres per second (middle), and the raw Sentinel-1 derived flood extent (bottom). The comparison validates that satellite-derived flooding estimates peak at a similar time to when nearby river water levels peaked.

Figure S2.3 Sentinel-2 optical imagery overlaid with flood extent areas derived from Sentinel-1 SAR data

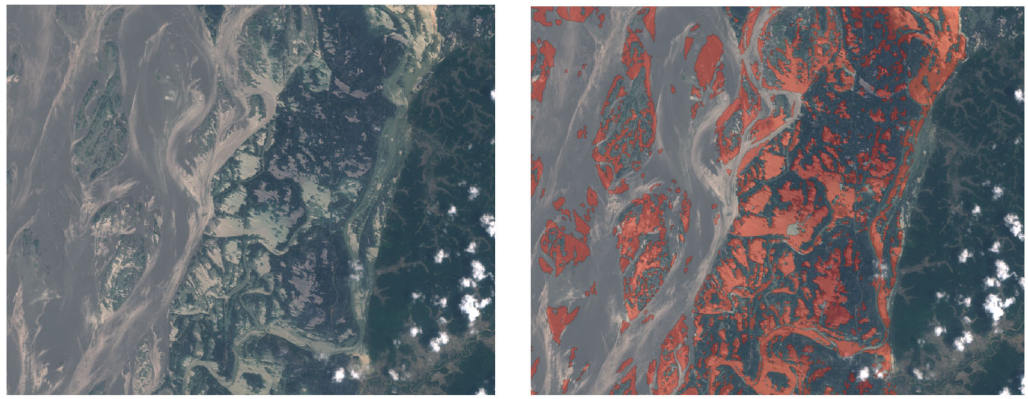

Source: Figure created by Hannah Ker (MapAction) on behalf of the Centre for Humanitarian Data, Office for the Coordination of Humanitarian Affairs, using Sentinel-1 SAR data and Sentinal-2 imagery.
Note: The figure shows two side-by-side images of the same area within the study region from 27 July 2020. The left panel shows Sentinel-2 optical imagery alone. The right panel overlays the Sentinel-1 derived flood extent areas in red on the same optical imagery. The close agreement between areas that appear flooded in the optical imagery and the red overlaid flood extents supports the validity of the Sentinel-1 derived flood mapping methodology.

S2.2.3. Comparison against key informant interviews from selected unions

We received survey data from key informants in 20 unions indicating their perceived flooding extent in their surrounding union. Each of these unions has data from 1–3 interview respondents. These data offer a useful comparison against our satellite-derived flooding estimates. Across these unions we see a general agreement in the flooding trend over time, and in many cases quite similar estimated magnitude, as shown in fig. S2.4.

Figure S2.4 Comparison between satellite-derived flooding estimates and those from key informants

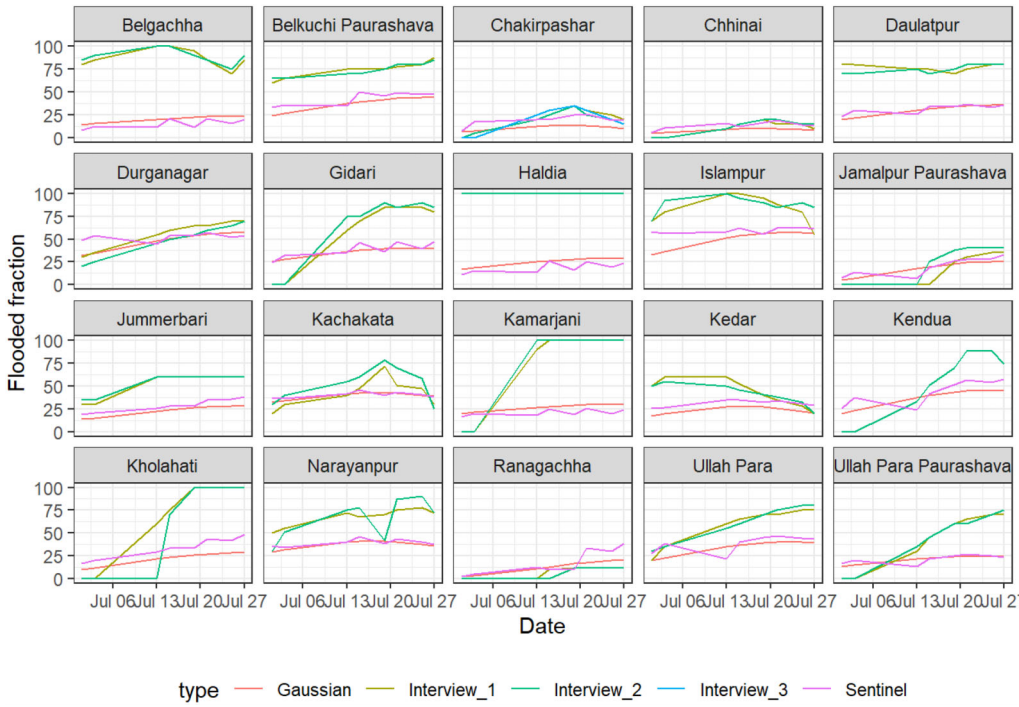

Source: Figure created by Hannah Ker (MapAction) on behalf of the Centre for Humanitarian Data, Office for the Coordination of Humanitarian Affairs, using Sentinel-1 SAR and survey data.
Note: The figure compares satellite-derived flooding estimates against perceived flooding extent reported by key informants in 20 unions, from 6 to 27 July 2020. Each panel corresponds to one union. Within each panel, lines show the Gaussian-smoothed flood extent, the raw Sentinel-1 derived flood extent, and the perceived flooding extent from up to three interview respondents. The vertical axis shows flooded fraction and the horizontal axis shows dates.

S3. Additional analysis in our preanalysis plan

S3.1. Heterogeneity by land type

In our preanalysis plan, we prespecified exploring heterogeneity by land type—a potential targeting tool, as it is easily observed. We categorized the 639 mauzas into three increasingly flood-prone categories using spatial data on the Jamuna River and 800 km of flood embankments: (a) protected or embanked mainland; (b) unprotected mainland outside embankments; and (c) char lands (low-lying islands formed by riverine silt deposits). Roughly one-third of the sample falls into each category.

Table S3.1. Heterogeneityby land type

	(1) Child food consumption	(2) Adult-food-consumption index	(3) Life satis-faction	(4) Pre-emptive actions	(5) Asset loss index	(6) Borrowing index	(7) Remit-tances	(8) Earning-potential index
Intent-to-treat (ITT) effect	0.141**	0.052	0.252***	0.058	−0.134***	−0.038	0.072	0.004
	(0.055)	(0.053)	(0.046)	(0.047)	(0.049)	(0.058)	(0.052)	(0.050)
Char	0.015	−0.171**	0.130**	−0.062	−0.025	−0.025	−0.016	−0.137**
	(0.075)	(0.068)	(0.064)	(0.067)	(0.068)	(0.075)	(0.072)	(0.066)
ITT × char	−0.053	−0.025	−0.200***	0.002	0.016	0.024	−0.026	0.134**
	(0.072)	(0.066)	(0.064)	(0.062)	(0.067)	(0.074)	(0.068)	(0.063)
Protected	0.082	−0.075	0.042	−0.052	−0.169**	0.074	0.117*	−0.006
	(0.078)	(0.072)	(0.068)	(0.070)	(0.068)	(0.081)	(0.071)	(0.070)
ITT × protected	−0.112	−0.036	0.020	0.028	0.095	−0.061	−0.097	0.081
	(0.075)	(0.071)	(0.070)	(0.066)	(0.064)	(0.081)	(0.071)	(0.069)
Treat effect: Char	0.087*	0.027	0.052	0.061	-0.118**	−0.014	0.046	0.139***
Treat effect: Protected	0.028	0.017	0.272***	0.087*	−0.040	−0.099*	−0.025	0.086*
p-value: Char = Prot.	0.394	0.866	0.001	0.674	0.198	0.243	0.275	0.385
F-test *p*-value:								
Control $\Delta = 0$	0.514	0.037	0.123	0.617	0.024	0.422	0.105	0.050
Treatment $\Delta = 0$	0.321	0.878	0.001	0.889	0.257	0.500	0.352	0.106
Controls	✓	✓	✓	✓	✓	✓	✓	✓
Union fixed effects	✓	✓	✓	✓	✓	✓	✓	✓
N	7,631	9,034	9,023	9,030	9,033	6,104	9,033	9,027
R^2	0.04	0.09	0.10	0.10	0.13	0.09	0.04	0.11

Source: Authors' analysis based on survey data.
Note: The table reports the standardized mean treatment effect for each outcome estimated using the main specification. The treatment variable is interacted with each category of land type where the household is located, where the baseline is unprotected mainland. Covariates include age, gender, education level, household size, dependency ratio, and house structure. Union fixed effects are included. $^{*}p < 0.10$, $^{**}p < 0.05$, $^{***}p < 0.01$.

S3.2. Alternative specification for transfer timing

In the preanalysis plan, we prespecified an alternative model comparing households that were identified to receive the cash transfer on 14, 15, and 16 July to households that were identified to receive the transfer on 30 July.

Table S3.2. Treatment effects by timing of transfer, 14–16 July versus 30 July

	(1) Child food consumption	(2) Adult-food-consumption index	(3) Life satis-faction	(4) Pre-emptive actions	(5) Asset loss index	(6) Borrowing index	(7) Remit-tances	(8) Earning-potential index
Transfer on	0.087***	0.040	0.174***	0.078***	−0.093***	−0.031	0.030	0.078***
14–16 July	(0.031)	(0.028)	(0.029)	(0.026)	(0.028)	(0.032)	(0.029)	(0.027)
Transfer on 30	0.072	−0.032	0.207***	−0.004	−0.144***	−0.154***	0.046	0.121***
July	(0.048)	(0.042)	(0.045)	(0.039)	(0.041)	(0.046)	(0.048)	(0.041)
q-value: 14–16 July	0.009	0.133	0.001	0.008	0.004	0.273	0.261	0.008
q-value: 30 July	0.129	0.295	0.001	0.512	0.004	0.004	0.273	0.008
p-value: 14–16 July = 30 July	0.728	0.052	0.416	0.014	0.133	0.002	0.716	0.226
q-value: 14–16 July = 30 July	0.399	0.060	0.295	0.019	0.129	0.006	0.399	0.204
Controls	✓	✓	✓	✓	✓	✓	✓	✓
Union fixed effects	✓	✓	✓	✓	✓	✓	✓	✓
N	7,631	9,034	9,023	9,030	9,033	6,104	9,033	9,027
R^2	0.04	0.09	0.10	0.10	0.13	0.09	0.04	0.11

Source: Authors' analysis based on survey data.
Note: The table reports the standardized mean treatment effects for transfers made on 14–16 July and for transfers made on 30 July. We report the *p*-value from a test that treatment effects are equal, and false discovery rate *q*-values across the eight outcomes for each timing of the transfer respectively. We control for the same covariates and union fixed effects used in the main analysis. $^{*}p < 0.10$, $^{**}p < 0.05$, $^{***}p < 0.01$.

S4. Additional supplementary tables

Table S4.1. Balance table of socioeconomic characteristics (five-month follow-up survey)

	(1) No transfer Mean	(2) Transfer Mean	(1) − (2) Difference (Union FE)	(1) − (2) Difference (Mauza FE)
Individual and household characteristics				
Age	37.246	37.011	0.235	0.235
Female respondent	0.977	0.989	−0.012	−0.012
Household head	0.264	0.233	0.031	0.031
No schooling	0.487	0.416	0.072*	0.072*
Completed primary school	0.341	0.422	−0.081	−0.081
Completed middle school	0.108	0.196	−0.088**	−0.088**
Completed high school	0.020	0.044	−0.024	−0.024
Household size	4.511	4.578	−0.066	−0.066
Number of people less than 6 years old	1.585	1.527	0.058	0.058
Number of people at least 60 years old	0.391	0.430	−0.039	−0.039
Dependency ratio	0.785	0.745	0.039	0.039
Raw material house	0.279	0.200	0.079	0.079
Tin walls and roof house	0.709	0.790	−0.080	−0.080*
Tin/brick house	0.010	0.008	0.002	0.002
Technology use				
Used digital wallet in last six months	0.598	0.540	0.058*	0.058
Own mobile	0.864	0.874	−0.010	−0.010
Uses someone else's mobile	0.127	0.122	0.005	0.005
Uses mobile at least once a week	0.982	0.991	−0.008	−0.008
Anticipatory action interventions				
Received World Food Programme transfer (self-report)	0.000	0.937	−0.937***	−0.937***
Number of observations	788	746	1,534	1,534

Source: Authors' analysis based on survey data.
Note: The table reports mean values of individual and household characteristics that are likely to be time invariant, and descriptive statistics on technology use and self-reported receipt of anticipatory action interventions from the World Food Programme, United Nations Population Fund and Food and Agriculture Organization. The last two columns report the difference in means from ordinary least squares regressions of each variable on the treatment dummy, controlling for union fixed effects in column three, and mauza fixed effects in column four as in our main specification. Robust standard errors were used to correct for heteroskedasticity. $^{*}p < 0.10$, $^{**}p < 0.05$, $^{***}p < 0.01$.

Table S4.2. Lee bounds to correct for differential attrition

	Standardized mean treatment effect [*N*]	**Call received Δ nonresponse rate = 4.3 percent [*N*]**
Child food consumption	0.101***	0.101***/0.101***
	[7,541]	[7,541/7,541]
Adult-food-consumption index	0.037	−0.060**/0.095***
	[8,948]	[8,658/8,652]
Life satisfaction	0.178***	0.048*/0.178***
	[8,937]	[8,691/8,937]
Preemptive actions	0.075***	0.045*/0.075***
	[8,944]	[8,832/8,944]
Asset loss index	−0.074***	−0.184***/−0.074***
	[8,947]	[8,671/8,947]
Costly borrowing index	−0.049	−0.152***/−0.034
	[5,996]	[5,805/5,943]
Remittances	0.041	0.041/0.041
	[8,947]	[8,947/8,947]
Earning-potential index	0.051*	−0.051*/0.051*
	[8,941]	[8,655/8,941]

Source: Authors' analysis based on survey data.
Note: Lee (2009) bounds (lower/upper) for estimated treatment effects are shown for differential nonresponse rate of 4.3 percent, conditional on a call being received. Higher nonresponse was recorded in the control group. Covariates include age, gender, education level, household size, dependency ratio, house structure, recipient status for United Nations Population Fund and Food and Agriculture Organization-led interventions, and land type. Mauza fixed effects are included. Standard errors are clustered at union level for inference. The numbers of observations included when calculating high and low bounds are shown in square brackets. $^{*}p < 0.10$, $^{**}p < 0.05$, $^{***}p < 0.01$.